frontiers | Frontiers in Materials

TYPE Original Research
PUBLISHED 06 September 2022
DOI 10.3389/fmats.2022.980887

OPEN ACCESS

EDITED BY
Yue Zhang,
Qingdao University of Technology, China

REVIEWED BY
Haoliang Huang,
South China University of Technology, China
Piotr Smarzewski,
Lublin University of Technology, Poland
Jing Zhong,
Harbin Institute of Technology, China

*CORRESPONDENCE
Jinrui Zhang,
jinrui.zhang@tju.edu.cn

SPECIALTY SECTION
This article was submitted to Computational Materials Science, a section of the journal Frontiers in Materials

RECEIVED 29 June 2022
ACCEPTED 11 August 2022
PUBLISHED 06 September 2022

CITATION
Zhu Y, Liu Y and Zhang J (2022), Monitoring the hydration behavior of hardened cement paste affected by different environmental pH regimes. *Front. Mater.* 9:980887.
doi: 10.3389/fmats.2022.980887

Monitoring the hydration behavior of hardened cement paste affected by different environmental pH regimes

Yu Zhu[1], Yijie Liu[1] and Jinrui Zhang[2]*

[1]Henan Key Laboratory of Materials on Deep-Earth Engineering, School of Materials Science and Engineering, Henan Polytechnic University, Jiaozuo, Henan, China, [2]State Key Laboratory of Hydraulic Engineering Simulation and Safety, Tianjin University, Tianjin, China

The purpose of this paper is to investigate the hydration behavior of hardened Portland cement paste cured in different environmental pH values by compressive strength, XRD, TG-DTG and EIS. Meanwhile, a newly proposed equivalent circuit model is built to establish the correlation between the electrochemical parameters and compressive strength of cement paste. The results show that the matrix strength, hydration products and pore structure of hardened cement paste are significantly affected by different pH values. According to the *in-situ* nondestructive monitoring of EIS, the evaluating for the matrix strength of cement-based materials can be achieved by calculating the resistivity of discontinuous connected pores (R_{cp}) in the recommended equivalent circuit model.

KEYWORDS

cement paste, pH value, compressive strength, EIS, hydration

1 Introduction

With the rapid development, industrial waste pollution and urban pollution are gradually expanding, which changes the environmental pH value, especially the pH of groundwater (Hernandez-Vargas et al., 2018). As the most widely building materials used in civil engineering, the cement-based materials are subjected to attack from groundwater. A variety of physical and chemical interactions occur between cement-based materials and the service environments, which may lead to decomposition of hydration products and defects in matrix structure, and further weaken the mechanical properties and durability of the building structures (Li et al., 2018).

There are lots of investigation about the macroscopic characteristics and pore structure of cement-based materials exposed to various aggressive environments (Bertron et al., 2005; Kazemian et al., 2011; Li et al., 2017a). The resistance to seawater corrosion of the cementitious systems has been studied and it is found that the decline in compressive strength is mainly due to the attacks of chloride, sulfate, and magnesium ions in seawater (Li et al., 2017b). In addition, Yimmy Fernando Silva et al. had investigated the replacement of Portland cement by the residue of masonry in self-compacting concrete to improve the resistance to sulfates (Na_2SO_4 and $MgSO_4$), a

decrease of more than 50% in expansion and less degradation of the compressive strength, caused by lower content of C_3A (Silva and Delvasto, 2021).

The commonly used methods for measuring the pore structure of cementitious materials are mercury intrusion porosimetry (MIP) and nitrogen adsorption (BET). However, the above methods should require the specimen destruction and only reflect the pore structure characteristics of the small part in specimen, not the whole pore structure. Therefore, in this paper, in order to effectively reflect the changes of the whole sample structure, the electrochemical impedance spectroscopy (EIS) method are introduced to the study of pore structure changes in cementitious materials.

As a nondestructive monitoring method, EIS method can be used to characterize the internal microstructure of cementitious materials and effectively evaluate the mechanical properties, permeability and durability of concrete (Jain and Neithalath, 2011; Ortega et al., 2015; He et al., 2018). Meanwhile, the method can effectively avoid the effects of local sampling and pretreatment on the microstructure of specimens (Diamond, 2000a; Lloyd et al., 2009; Thomas et al., 2011; Ismail et al., 2013; He et al., 2018). There are lots of investigation about the effect of water-cement ratio and mineral admixtures on the internal conductivity and capacitance parameters in the cement system by EIS (Dong et al., 2016; Dong et al., 2019; Hassi et al., 2020). Additionally, the effect of mineral admixtures on the durability of cement mortars was conducted by EIS (Hassi et al., 2020). The experimental results showed that the addition of 10% fly ash and 10% silica fume could increase the corrosion resistance under the chloride ions (Hassi et al., 2020). The characterization of carbonation behavior of fly ash blended cement materials also was studied by the electrochemical impedance spectroscopy method (Dong et al., 2016). The functional relationship has been built among the fitted parameters of the model and the carbonation time and predicted the carbonation depth of fly ash bended cement materials (Song, 2000; Cruz et al., 2013; Hu et al., 2019).

Based on EIS analysis, the relationship has been established between the compressive strength and the electrochemical parameters (R_s and R_{ct}) of hardened cement pastes, Biqin Dong (Dong et al., 2017) found that the electrochemical impedance spectrum parameter R_{ct1} had a similar growth trend with compressive strength, and established a relationship between compressive strength and R_{ct1}. Additionally, Chi (Chi et al., 2019) established a clear linear relationship between the impedance logarithm measured by EIS and the compressive strength of cement slurry. The numerical equation of resistivity and strength was established by Gusheng Wei (Wei et al., 2012). By measuring the resistivity of cement within 24 h, the standard strength of unknown cement within 28 days was determined. Tiantian Guo (Guo et al., 2021) found that the compressive strength showed a similar trend to the impedance parameter R_s, the correlation between R_s and compressive strength can be fitted by a linear equation. but few investigations have referred the relationship between the resistivity of discontinuous connected pores (R_{cp}) and the compressive strength. Therefore, in this paper, the mathematical relation between the discontinuous pore and strength will be analyzed.

The purpose of this paper is to investigate the effect of different environmental pH values on the hydration behaviors of hardened Portland cement paste by *in-situ* nondestructive monitoring method (EIS), so as to realize the prediction of the matrix strength of cementitious materials. In this paper, the hardened cement paste is firstly prepared and cured in different environmental pH values. Then, the compressive strength, X-ray diffraction (XRD), thermal analysis (TG-DTG) and EIS are conducted to study the performance, phase analysis and pore structure of Portland cement paste. Finally, a new equivalent circuit is proposed to build the quantitative relation between matrix strength and the calculated discontinuous pores.

2 Experimental programs

2.1 Materials

In this paper, Portland cement (P.I 42.5R) was obtained from Shandong Lucheng cement Co., Ltd. The phase compositions were presented in Table 1, respectively. The sodium hydroxide (NaOH) purchased has a purity of 96%, with white granular. The hydrochloric acid (HCl) was manufactured with a content of 36%–38%, and density of 1.18 g/ml.

2.2 Paste preparation

All cement pastes were prepared at a constant water-cement ratio of 0.4. The fresh cement pastes were cast into the mold with the size of 20 × 20 × 20 mm and cured at 20 ± 2°C and RH of 95 ± 5% for 24 h. After demolding, the prepared specimens were immersed in three different curing environments (pH = 3, 7 and 12) until the required age for testing.

2.3 Test methods for cement paste

2.3.1 Compressive strength test

The compressive strength was measured at 1, 3, 7 and 28 days by the microcomputer-controlled electronic universal testing machine (WDW-300) with a uniform loading rate of 0.2 mm/min. The average of six samples with the size of 20 × 20 × 20 mm was the measured compressive strength at the tested age.

TABLE 1 The chemical compositions of the Portland cement/wt%.

SiO_2	Al_2O_3	Fe_2O_3	CaO	MgO	Na_2O	SO_3	*f*-CaO	Loss	Cl^-
21.88	4.49	3.45	64.65	2.36	0.51	2.44	0.9	1.25	0.01

2.3.2 X-ray diffraction

The hardened cement pastes were broken into small pieces and then immersed in anhydrous ethanol for 24 h to terminate the hydration process. The crushed cement paste pieces were further ground into powder with a particle size smaller than 80 μm and dried in a vacuum oven at temperature of 60°C. The cement powders were characterized by XRD (RigakuD/max2550) with a scan rate of 10°/min and 5–85° (2θ) scanning range.

2.3.3 Electrochemical impedance spectroscopy

After the cement paste was poured into the plastic mold, two electrode sheets were fixed in the paste and connected to the test apparatus. The EIS measurements were conducted via a PARSTAT 2273 Electrochemical Workstation with an AC voltage of 30 mv, using the frequency range from 1 Hz to 1 MHz.

2.3.4 Thermal analysis (TG-DTG)

The dried cement pastes were ground into powder with a particle size of less than 75 μm. A comprehensive thermal analyzer (BJ-HCT-3) was used to carry out thermal analysis on approximately 15 mg of powder samples, which was heated from 20 to 1,000°C at a rate of 10°C/min under a nitrogen atmosphere.

2.3.5 Ultra depth of field microscope

The samples cured at 28 days were soaked in ethanol for 24 h to terminate hydration. The samples were dried in a vacuum dryer for 24 h until their mass was constant. Ultra-depth of field microscope (Leica DVM6) was used to observe the pore structure of samples at 100 times magnification.

2.3.6 Scanning electrical microscopy

The sampling method is the same as the super-depth of field test. After the dried samples are sprayed with gold, the microstructure of the bulk samples is observed by a Merlin Compact field emission scanning electron microscope manufactured by Carl Zeiss NTS GmbH, Germany.

3 Results and discussion

3.1 Compressive strength

Figure 1 shows the influence of different pH values on the compressive strength of hardened Portland cement. The test results show that the compressive strength of all samples

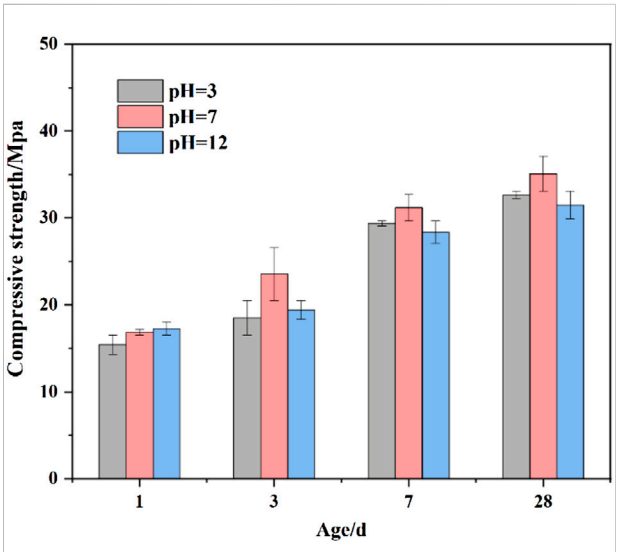

FIGURE 1
Compressive strength of cement pastes in different pH values.

increases significantly with the curing age due to the further hydration of the cementing material in the hardened slurry. When the hydration age is 3 days, the compressive strength of (23 MPa) at pH = 7 is significantly higher than that at pH = 3 (18 MPa) and pH = 12 (19 MPa), and the influence of acidic erosion solution on the strength is more obvious. This is due to the fact that CH and C-S-H gels in the hydration products of silicate cement are the most vulnerable substances in the cement paste to be damaged by erosive media (De Windt and Devillers, 2010; Gutberlet et al., 2015; Yang et al., 2018; Muthu et al., 2021).

On the one hand, CH is sensitive to acid, easy to have acid-base neutralization reaction with acid, quickly dissolve in acidic environment; The stable existence of C-S-H depends on alkaline environment with pH higher than 12.4 (Renaudin et al., 2009; De Weerdt and Justnes, 2015; Liu et al., 2021). On the other hand, the degradation of C-S-H structure was aggravated by the continuous decrease of basicity of pore solution caused by the consumption of CH. The loss of CH and decomposition of C-S-H lead to the continuous increase of the porosity of cement slurry, resulting in the formation of relatively loose microstructure, and the decline of mechanical properties of cement slurry. However, in the alkaline erosion environment, after cement hydration (3 days), the alkali in the solution rapidly dissolves into the

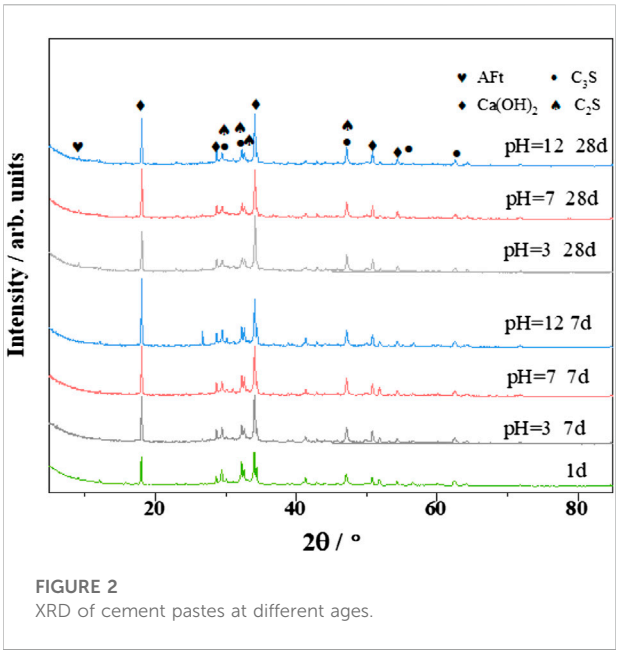

FIGURE 2
XRD of cement pastes at different ages.

liquid phase. Since the nucleation of CH is controlled by its solubility product K_{CH} ($K_{CH} = [Ca^{2+}]\,[OH^-]$), the additional OH^- can nucleate CH rapidly and precipitate, resulting in the decrease of Ca^{2+} in the solution and promoting the reaction (1). (2) To the right to accelerate the hydration of cement clinker minerals C_3A and C_3S (Shayan, 1989; Dove, 1999; Xue et al., 2022). The crystallization growth of hydration products such as C-S-H, $Ca(OH)_2$ and AFt was promoted. A large number of generated hydration products make the pores of the slurry filled (Grutzeck, 1999). However, due to the excessive and rapid generation of hydration products in the early stage, the distribution of the products is uneven, resulting in the reduction of the compressive strength of the cement in the early stage of hydration.

$$C_3S + 5.3H \rightarrow C_{1.7}SH_4 + 1.3CH \quad (1)$$

$$C_2S + 4.3H \rightarrow C_{1.7}SH_4 + 0.3CH \quad (2)$$

At the later stage of hydration (7–28 days), compared with the specimens with pH value of 7, the matrix strength of pH 3 and 12 hardened cement paste decreased more slowly compared to the early stage by 6.4% and 9.67%, respectively. The effect of alkaline conditions on the later compressive strength of the cement is even more. This may be due to the fact that OPC contains a large amount of CH inside, thus promoting the formation of calcium alumina from C_3A and $CaSO_4{\cdot}2H_2O$ (Wang et al., 2016), Causes a continuous increase in the volume of the solid phase, generating a continuous increase in the crystallization pressure in the internal micropores of the cement paste, which results in significant cracks inside the specimen and eventually leads to a decrease in the strength of the cement paste under alkaline conditions of erosion. The pH value of pore solution has an effect on the stability of AFt, and the addition of alkali promotes the transformation of AFt into AFm (Tteardon, 1994; De Windt and Devillers, 2010).

3.2 XRD

Figure 2 shows the XRD patterns of Portland cement samples exposed to solutions of different pH values. There are significant differences in phase content of erosion products under different curing environments and erosion ages. In the early stage of cement hydration, C_3S and C_2S are gradually consumed to produce a small amount of AFt and $Ca(OH)_2$ (Shimada and Young, 2004).

As shown in Figure 2, the diffraction peaks of dicalcium silicate and tricalcium silicate are weaker than those of cement slurry in alkaline environment, which indicates that alkaline environment can promote the hydration process of cement. The content of CH reached the maximum at 7 days, while at 28 days of hydration, the diffraction peak of CH decreased significantly in alkaline environment, The CH content reached the maximum at 7 days, while the diffraction peak of CH in alkaline environment decreased significantly when the hydration age reached 28 days. The diffraction peak of AFm gradually appeared, indicating that CH was gradually consumed in the late stage of hydration, resulting in the gradual conversion of AFt to AFm.

In order to better analyze the effect of pH on the hydration products of the hardened cement paste, the diffraction peaks of the cement hydration products CH and AFt are plotted in this paper. Figure 3 shows the diffraction peaks of CH on (001), (100), (101) and (102) crystal planes at different angles (18.12°, 28.77°, 34.17°, 50.88°). As can be seen from the figure, the characteristic peak of CH shifted to the left with the increase of pH value, which indicates that the nucleation of CH crystal can be promoted in the hardened cement slurry cured at pH = 7 and 12, resulting in the increase of the size of CH crystal. At the same time, it is found that the diffraction peak of CH increases gradually with the increase of pH value, which further indicates that CH is easily consumed by H^+ under acidic conditions (Mohit et al., 2021).

It can be found that several major diffraction peaks of AFt are shifted to the left at pH = 12. This indicates that the alkaline environment can induce a larger spacing between the crystalline surfaces of AFt, an increase in the aspect ratio of AFt, and a morphological shift from columnar to fine needle-like (Ramachandran et al., 1993). The stability of chalcocite also decreases in strong alkaline environments (Juenger and Jennings, 2001a; Wang et al., 2016), which is responsible for the decrease in the intensity of its diffraction peaks. Since the shifts of CH and AFt are different, the case that all diffraction peaks are shifted due

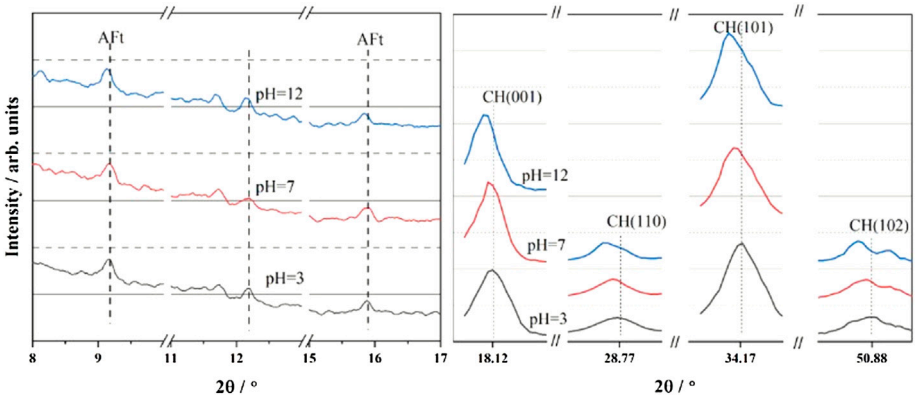

FIGURE 3
CH and AFt diffraction peak in Silicate cement paste (28 days).

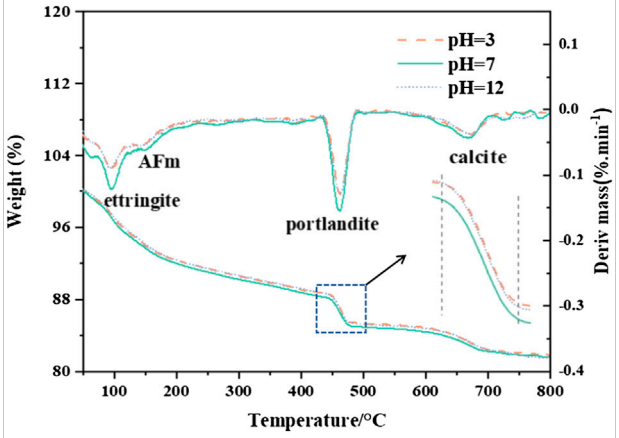

FIGURE 4
TG-DTG curves of hardened cement pastes.

to experimental errors can be excluded, thus it can be inferred that the shifts are caused by the morphological changes of hydration products.

3.3 TG-DTG

Figure 4 shows the TG-DTG curves of hardened silicate cement slurry at different pH values. TG-DTG curve showed that AFt and CH were generated in the hydration process of OPC, and mass loss of $CaCO_3$ appeared on the curve due to partial carbonization of calcium hydroxide. It should be noted that a large number of C-S-H decomposition of gel products can be carried out in the whole test temperature range, so there is no obvious horizontal segment in the TG curve of hydrated samples. As shown in Figure 4, it can be clearly observed that when the hydration time is 28 days, the TG curve obviously shows a weightlessness peak of AFm, indicating that AFt is partially converted into AFm in the late hydration period.

To further investigate the effect of different pH values on the hardened cement paste, the main products of the hardened cement paste were quantified based on the TG-DTG curve as shown in Table 2.

It is noted that Ca(OH)#2 is a chemical substance of the matrix itself. Ca(OH)*₂ is converted from $CaCO_3$. The total amount of $Ca(OH)_2$ is the sum of $Ca(OH)_2^{\#}$ and Ca(OH)*₂

As can be seen from Table 2, AFt content in cement paste increased rapidly on 1d, which was due to the rapid reaction between C_3A in cement and gypsum, resulting in a large amount of AFt. As the curing age prolongs, AFt content changes from 12.506% at 1d to about 8.50% at 3 days, which is because after a period of cement hydration, the gypsum content in the cement system gradually decreases, and the generated AFt is gradually consumed by calcium aluminate (Zivica and Bajza, 2002). Moreover, the amount of AFt with pH = 12 decrease 10% compared to that with pH = 3, which is because NaOH can cause the instability of AFt at early age, which tends to produce monosulfide calcium sulphoaluminate (AFm).

When the hydration age is 3 days, the content of hydration products in hardened cement slurry with too high pH value (pH = 12) and too low pH value (pH = 3) is slightly more than that of neutral curing. When hydration age reaches 28 days, AFt content in acidic condition decreases compared with other curing environments, because $Ca(OH)_2$ not only improves the hardness and compactness of hardened cement slurry, but also provides an alkaline environment for stable AFt (Zivica and Bajza, 2002). When the pH value is 3, $Ca(OH)_2$ is prone to acid-base neutralization reaction with acid, resulting in a rapid decrease in $Ca(OH)_2$ content, so that AFt cannot be stabilized (Wang et al., 2016). In alkaline environment, the content of $Ca(OH)_2$ increased significantly, but the content of AFt decreased

TABLE 2 Content of cement hydration products in different curing environments/%.

Age/d	pH	AFt	$Ca(OH)^{\#}_2$	$CaCO_3$	$Ca(OH)^{*}_2$	Total $Ca(OH)_2$
1	---	9.756	11.799	5.943	4.402	16.201
	3	9.447	10.228	4.518	3.347	13.574
3	7	8.322	11.087	4.501	3.334	14.421
	12	8.366	11.497	4.562	3.380	14.876
	3	9.328	14.434	5.698	4.221	18.655
7	7	8.798	12.997	5.297	3.924	16.921
	12	9.281	13.147	7.062	5.231	18.378
	3	18.019	13.252	6.797	5.035	18.287
28	7	18.490	13.844	5.868	4.346	18.190
	12	18.395	14.082	6.450	4.778	18.860

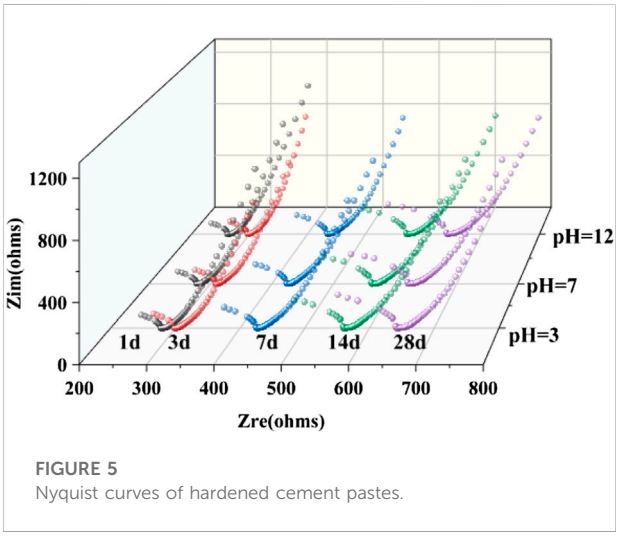

FIGURE 5
Nyquist curves of hardened cement pastes.

compared with that in neutral environment. This was because when the content of alkali increased, CH nucleation was promoted, but OH^- promoted the transformation of AFt into AFm, which reduced the content of AFt (Guo et al., 2022).

3.4 EIS

3.4.1 Nyquist plots

Figure 5 shows Nyquist diagram of Portland cement net slurry under curing at different pH values. As can be seen from Figure 5, Nyquist curves of hardened cement slurries all show obvious similar semi-arcs, and the radius of the arcs increases significantly with the increase of age. In addition, the intersection of the semicircle and the abscissa of the complex plane (the volume resistance of hardened paste) increases with the age. This is due to the increase of hydration time, cement hydration products gradually dense, hydration overall porosity gradually reduced.

Due to the extraction of relevant parameters from Nyquist diagram to obtain more pore network structure information, it is necessary to establish an appropriate electrochemical model. Therefore, the influence of pH value on Nyquist curve will be discussed in the next part combined with equivalent circuit and related electrochemical parameters.

3.4.2 Simulated equivalent circuit

The equivalent circuit method is widely used in the analysis and application of EIS in cement system (Ribeiro and Abrantes, 2016; Dong et al., 2017). The equivalent circuit consists of electrochemical elements such as capacitance, inductance and resistance in series and/or in parallel. Generally, the obtained electrochemical elements are used to analyze the characteristics of EIS of cement, so as to study the electrical properties and microstructure of cementitious materials (Song, 2000; Taylor et al., 2001).

The solid-liquid interface in cement system is considered as the interface between the hydration products and pore solution. It is referred that the heterogeneity of hydration products and the uneven charge space distribution in the matrix can lead to the change of electric double layer capacitance at the solid-liquid interface with frequency, resulting in the change of relaxation time in the impedance spectrum of cement paste and further "dispersion effect" (He et al., 2017). Therefore, as for EIS of cements system, its arc will shift. In this paper, based on the equivalent circuit built by Song (Song, 2000) and Cabeza (Cabeza et al., 2002), a novel equivalent circuit model is established by considering both the dispersion effect and the diffusion at the cement/electrode interface.

As illustrated in Figure 6, the equivalent circuit proposed in this paper adds Warburg diffusion element (W_1). Meanwhile, the double-layer capacitor (Q) is used to replace the parallel plate capacitor (C) in classical Randle model. Whereas, the double-layer capacitor can be used to characterize the dispersion effect between the electrode and the electrolyte, thus giving a true reflection of the polarization

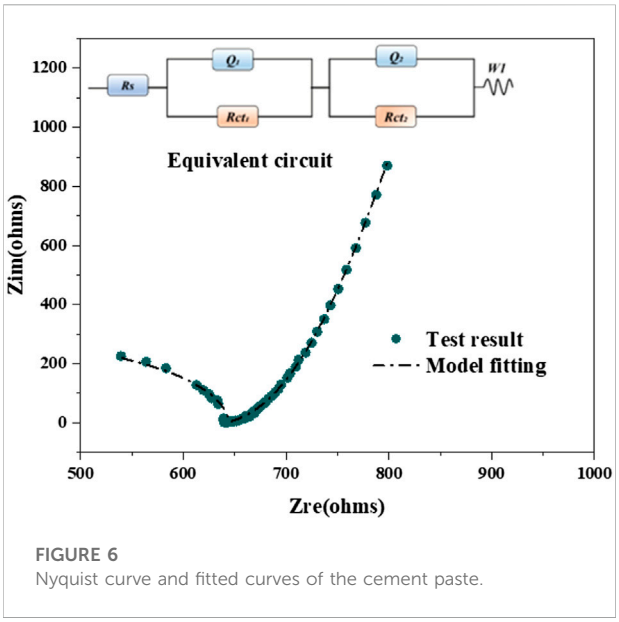

FIGURE 6
Nyquist curve and fitted curves of the cement paste.

process of the cement system. Additionally, in the early stages of hydration of Portland cements, although the hydration degree is low, the concentration of ions in the pore solution of the cement paste is high. Meanwhile, there is a significant diffusion of pore solution ions as well as "free water". Therefore, it is necessary to employ the Warburg diffusion element (W_1) to reflect the characteristics of cement hydration at early ages.

As shown in Figure 6, the equivalent circuit includes: solution resistance (R_s), charge transfer resistance (R_{ct}), double layer capacitance (Q) and Warburgresistance (W_1). Whereas, R_s represents the resistance generated by the electrolyte solution within the pores of the hardened cement paste; R_{ct} refers to the resistance generated by the charge transfer process; Q_1 is the double layer capacitance present between the solid/liquid phase, Q_2 is the double layer between the cement and the electrode capacitance; W_1 is the Warburg resistance caused by the ion diffusion process within the cement.

In order to verify the validity of the equivalent circuit model proposed in this paper, the Nyquist curve is fitted by ZSimpWin software. It can be seen that the newly built model of $R_s(Q_1R_{ct1})(Q_2R_{ct2})$ W_1 is consistent with the high- and low-frequency regions of the measured EIS curve, which indicates that the equivalent circuit can be used to describe the changes of microstructure in cement system.

3.4.3 Calculated electrochemical parameters

The variation trend of different parameters in EIS can reflect the density and pore network structure of hardened cement slurry (Cabeza et al., 2002; Wilińska and Pacewska, 2018). R_s and R_{ct} are sensitive to the change of cement-based microstructure, so the above two parameters are selected to discuss the change of microstructure during cement hydration. Based on the equivalent circuit proposed in this paper, the curve of electrochemical parameters was fitted by Zsimpwin software.

It is known that R_s describes the resistance of the electrolyte in the pore solution of the hardened cement pastes. R_s is inversely proportional to the total concentration of ions in the pore solution (OH^-, K^+, Ca^{2+}, SO_4^{2-} and so on)and the total porosity of the paste (Zhu et al., 2017). In other words, the larger the R_s value, the less ions in the pore solution and the lower the total porosity of the matrix. Therefore, the lower value of R_s at early ages is attributed to the total amount of ions in the pore solution reaching the maximum. Additionally, the solid-liquid interface in cement system has just been formed to the extent that it is not yet thick enough, there are many pores and the total porosity is high in matrix, which also result in the lower R_s value at 1 and 3 days. As the curing age prolongs, a large number of ions participate in the reaction to produce hydration products, and further the macro pores are less and less, and the matrix structure is more and more dense. Therefore, the value of R_s increase obviously with the increase of curing age.

It can be seen from the Rct change curve in Figure 7 that the change of cement microstructure has a significant impact on R_{ct}. R_{ct} reflects the resistance of charge transfer reaction of hydrated electrons, which is inversely proportional to the number of hydrated electrons in the gel and the ion concentration in the pore solution.

When the hydration age is between 1 and 14 days, as conductive ions are constantly consumed in the hydration process of OPC, the hydration products rapidly occupy the internal pores of cement materials, resulting in a denser microstructure, which makes ion transfer more difficult and R_{ct} increases rapidly. By comparing the growth trend of Rct in different curing environments, it was found that R_{ct} showed a decreasing trend with the increase of pH value. The R_{ct} values of samples cured in acidic environment (119.28 Ω m) were significantly higher than those of the other two groups (126.84 Ω m and 126.84 Ω m). However, according to the quantitative analysis of hydration products mentioned above, H^+ infiltration into the cement sample is easy to react with CH, leading to the decalcification of C-S-H, the final cement structure is relatively loose and porosity increases, and the R_{ct} value should theoretically be lower than the other two groups. However, in an acidic environment, H^+ will react with OH^- ions in the solution to reduce the concentration of OH^- ions, so that the concentration of ions in the solution decreases. This indicates that R_{ct} value is influenced by ion concentration and pore structure of material. However, the R_{ct} value of the test block curing in alkaline environment at 28d decreased from 115.86 to 115.18 Ω, with a small decrease, but the R_{ct} value of the other two groups increased by about 20% compared with that at 14 days. This is because the fact that in an alkaline environment, AFt is formed in a solid phase reaction with agglomerated and

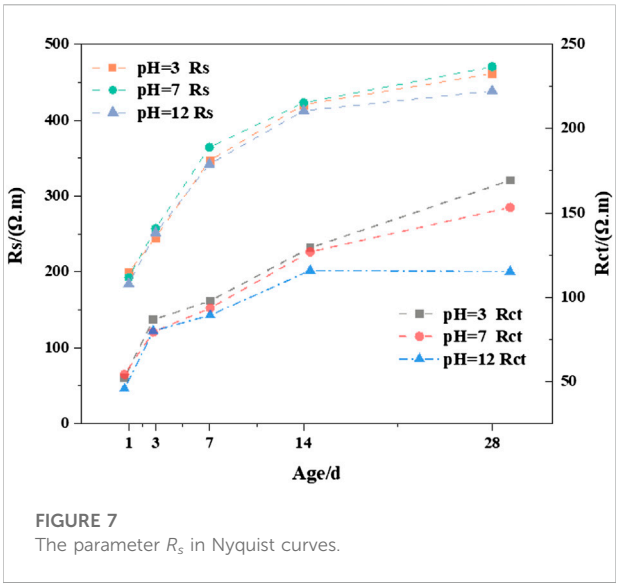

FIGURE 7
The parameter R_s in Nyquist curves.

outwardly radiating needle-like crystals. The crystals have a large specific surface area and cross-extrude each other, resulting in greater swelling stresses and internal microcracking of the cement specimens, which is consistent with the reduction of compressive strength.

3.4.4 Relation between EIS parameters and compressive strength

R_s and R_{ct} can be used to characterize the total porosity of the microstructure of cement system and the ion concentration of pore solution. However, the transmission characteristics of cement matrix are network structure formed by a variety of conductive paths formed by pores. In order to build the relation between the compressive strength between the pore network, the possible pore network in cement system should be considered. As shown in Figure 8, the pore network can be classified into three categories: (1) Continuously connected conductive path (consists of a series of capillaries connected continuously through an aperture, referred to as CCP, whose resistivity is denoted as R_{ccp}), (2) Discontinuous connected conductive path (consisting of discontinuous micropores continuously blocked by a cement matrix, referred to as DCP, whose resistivity is expressed as R_{cp}), (3) Insulation path (the path of formation of dense continuous matrix formed by hydration products and unhydrated cement, referred to as ICP) (Song, 2000; Kong et al., 2015; Hu et al., 2019).

It is known that the conductivity of ions in pore solution depends on the resistance both the continuous connected pores ($R_{ccp} = R_s + R_{ct}$) and discontinuous pores ($R_{cp} = R_{ccp} \times R_1/(R_{ct}\text{-}R_s)$). Whereas, R_s and R_{ct} are calculated from real impedance values for the left and right intersections of the semicircle and x axis, respectively, in accordance with equation $R = Z \times (A/L)$, where A and L are the sample area and length, perpendicular and parallel to the direction of the applied current, respectively (Spragg et al., 2014; Kong et al., 2016; Ramu et al., 2021).

Figure 9 displays the effect of environmental pH value on calculated parameter of R_{ccp} and R_{cp} as a function of curing age. As expected, the value of R_{ccp} increases with the age. However, the resistance value R_{ccp} decreases with the increasing pH, especially at the later ages. For examples, when the age curing age is 1d, the values of R_{ccp} with pH = 3, 7 and 12 is 280 Ω m, 276 Ω m and 260 Ω m. R_{ccp} at 28 days is 645 Ω m, 620 Ω m and 540 Ω m.

The reason why pH has a significant effect on R_{ccp} can be explained from two aspects. On the one hand, with the increase of pH value, the total amount of OH^- ions gradually increased. Snyder et al. believed that OH- was the main conductive ion in the pore solution of cementable materials. The reduction of hydroxyl group would lead to the increase of electromigration, making the ion transport through the pore easier and the value of R_{ccp} lower (Kong et al., 2015). On the other hand, in alkaline solution (pH = 12), excessive OH^- promotes the hydration process of cement, and the hydration products are generated too much and too fast, so that the products are not evenly distributed among each other, and more early hydration products wrap the unhydrated particles, which hinders the

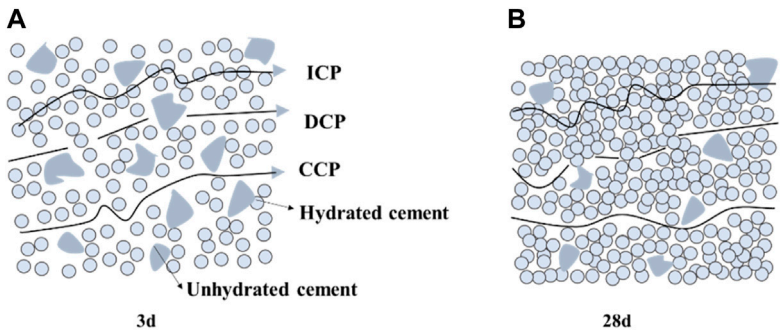

FIGURE 8
Schematic illustration of pore network in cement system.

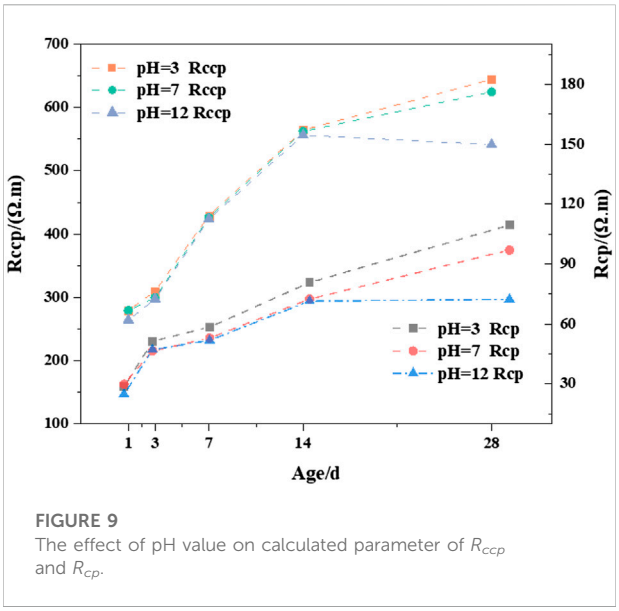

FIGURE 9
The effect of pH value on calculated parameter of R_{ccp} and R_{cp}.

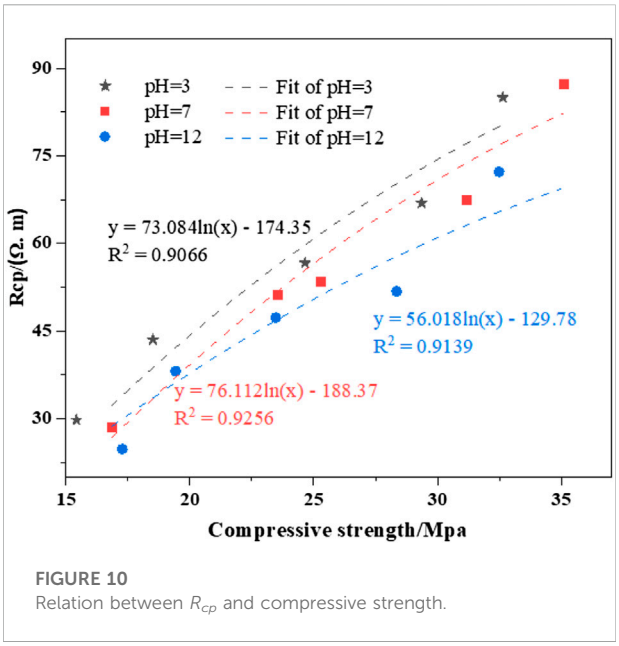

FIGURE 10
Relation between R_{cp} and compressive strength.

migration and diffusion of ions necessary for later hydration, thus reducing the connectivity of discontinuous conductive paths (the number of continuous holes increases), resulting in lower R_{ccp} values.

As shown in Figure 9, the trends of R_{cp} is similar to that of R_{ccp}. It should be noted that both R_{ccp} and R_{cp} with pH = 12 at 28 days decrease compared with the same specimens at 14 days. The reasons can be explained as follows: On the one hand, NaOH in the curing environment gradually penetrates into the matrix and reacts with CO_2 and H_2O to form $Na_2CO_3{\cdot}10H_2O$. The volume of $Na_2CO_3{\cdot}10H_2O$ is 2.5 times higher than that of NaOH. The internal expansion and internal stress are generated, resulting in microcracks, more continuous points, and gradually increasing connecting holes in the hardened cement. Finally, the matrix strength is weakening. On the other hand, at the later stage of hydration, with the increase of pH value in pore solution until the same as the environmental pH (pH = 12), NaOH can promote the transformation of AFt to single sulfur hydrated calcium sulphoaluminate (C_4ASH_{12}, AFm), following the reaction equations of (3) and (4) (Hu et al., 2019). The transformation from AFt to AFm leads to the increase of conductive ions and free water in newly generated hydration products, which can reduce the resistance (Snyder et al., 2003) R_{cp} and R_{ccp} (Tang et al., 2015).

$$C_3A + 3CSH_2 + 26H \rightarrow C_6AS_3H_{32} \quad (3)$$

$$C_6AS_3H_{32} + 4NaOH \rightarrow C_4ASH_{12} + 2Na_2SO_4 + 2CH + 20H \quad (4)$$

As known, the compressive strength is influenced by the pore structure in cement matrix (Paul et al., 2015; Tang et al., 2015; Yan et al., 2020). The magnitude of R_{ccp} and R_{cp} reflects to the evolution of the pore structure of the hardened cement paste, which may have a functional relationship with compressive strength. Therefore, in this paper, the parameter of R_{cp} and compressive strength are fitted, as shown in Figure 10. There is a logarithmic relationship between the compressive strength and R_{cp} of the cement paste. The fitted curves with pH = 3 and pH = 7 have similar trends.

The coefficient (R^2) of fit for R_{cp} and compressive strength is greater than 0.9066 for curves with different pH values. Therefore, the compressive strength of the cement at different ages can be well predicted by the value of R_{cp} with different environmental pH values.

3.5 Ultra depth of field microscope

Pore structure can reflect the phase composition and spatial morphology of cement hydration products to a certain extent. Figure 11 shows the pore structure characteristics of the slurry with different pH values.

The pore size increased significantly under the erosion of hydrochloric acid at pH 3, indicating that H^+ gradually consumed CH after entering the liquid phase, which reduced the basicity of pore solution, the stability of C-(A)-S-H gel and other aluminosilicates, and more calcium and aluminum ions dissolved in the acidic solution, resulting in the increase of harmful pores in the large pores (Gong and White, 2018). At the same time, combined with AFt peak shift in XRD, ettringite is more likely to crystallize into thick columns with the decrease of pH value of erosion solution, resulting in larger pores.

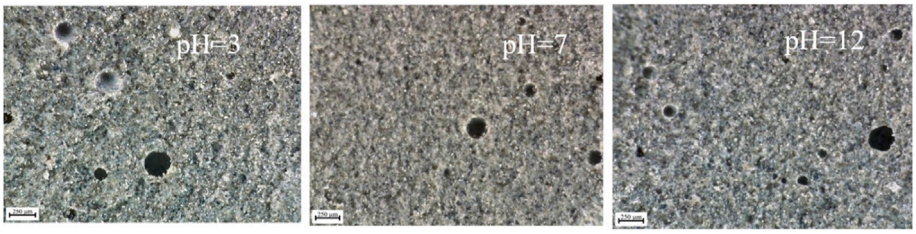

FIGURE 11
Superdepth of field of OPC hardened cement slurry.

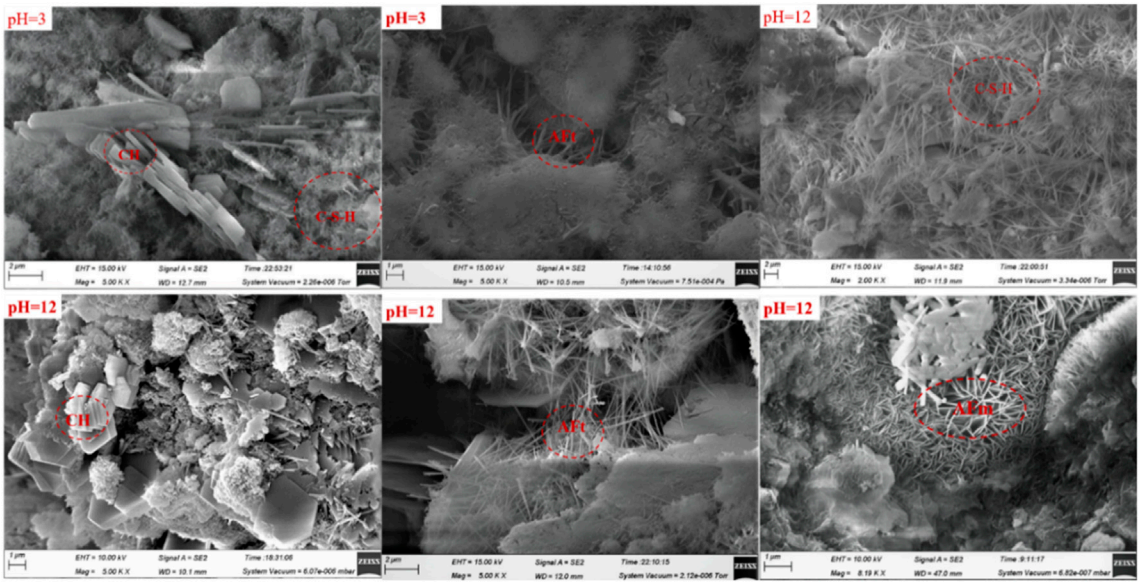

FIGURE 12
SEM image of OPC hardened cement paste (28 days).

It can be obviously found that the proportion of small pores increases significantly in the erosion of NaOH solution. This is due to the higher degree of supersaturation and faster nucleation of calcium hydroxide under alkaline conditions, which leads to larger CH crystal size and promotes higher CH crystallization in the cement slurry. The relatively dense structure of the cement slurry results in a decrease in total porosity and the number of macropores (Zhang et al., 2021), At the same time, Mori et al. 's study also showed that at the same hydration level, the addition of NaOH greatly reduced the BET specific surface area of the gel and the volume of gel pores (Okohira et al., 1974; Juenger and Jennings, 2001b). Moreover, OH^- can promote the gradual transformation of rod AFt into fine needle-like AFt, the growth of needle-like AFt can fill the pores and refine the pore size. However, at a later stage, the slurry structure is completely hardened and the pore structure is mature, the growth of AFt may lead to the expansion and cracking of the slurry structure, which has a negative impact on the strength.

3.6 SEM

To further illustrate the microstructural changes of OPC hydration pores and the reaction mechanism, the microstructure of cement hydration products $Ca(OH)_2$, C-S-H gel and ettringite were obtained from the image.

Figure 12 shows SEM images of cement slurry corroded in different pH solutions for 28 days. Cloudy C-S-H gels and well-crystallized ettringite columnar crystals were clearly observed in acid - eroded solution. This is because the decrease of the basicity

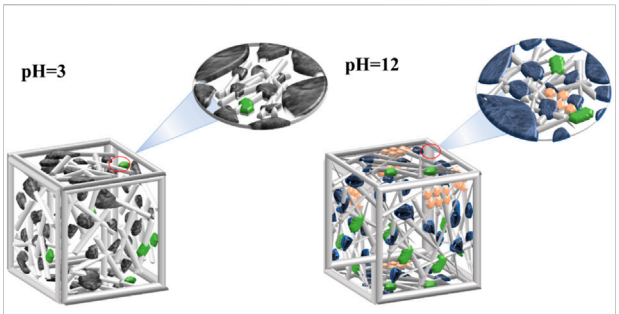

FIGURE 13
Hydration model of OPC hardened cement slurry.

of pore solution leads to the decalcification of C-S-H, and the decrease of Ca/Si ratio promotes the formation of cloudy C-S-H gel (Diamond, 2000b).

In alkaline solution, fibrous C-S-H gel and $Ca(OH)_2$ hexagonal plate-like crystal structure with significantly increased crystal size can be observed. This is due to the increase of crystallinity and change of morphology of C-S-H gels induced by alkali, which makes the microstructure of C-S-H gels coarse, forming flaky or fibrous gel hydration products and non-homogeneous state (Bentz, 2006). At the same time, due to the presence of a large amount of OH^- in the solution, OH^- can participate in the formation of ettringite crystal nuclei during the formation of ettringite, promoting the formation speed of crystal nuclei, so that the morphology of ettringite gradually changes from columnar to fine needle rod and grows radially outward with the increase of pH value (Zhang et al., 2017). Hexagonal lamellar AFm can be found under alkali erosion. This is due to the fact that alkali seems to reduce the stability of ettringite, and from Eqs 3, 4 it can be inferred that NaOH promotes the conversion of AFt to the monosulfur type hydrated sulfuric aluminate (Paglia et al., 2003).

Based on the microscopic test results of cement, the hydration model of Portland cement in different erosion solutions was established. It is worth noting that in Figure 13, the blue reticular gel substance is fibrous C-S-H, the gray gel substance represents cloudy C-S-H, the gray circular rod-shaped columnar substance represents columnar AFt, and the gray needle-like substance represents AFt, the green irregular crystal is $Ca(OH)_2$, and the red irregular crystal represents AFm.

4 Conclusion

In this paper, the influence of environmental pH value on hydration behavior of hardened cement paste are investigated by compressive strength, quantitative analysis of hydration products and the pore structure characteristics reflected by EIS parameters. The following conclusions can be obtained:

1) Both acidic and alkaline environments are detrimental to the strength development of hardened cement paste. The difference is that the acidic environment has a greater influence on the early strength of cement (1–3 days), while the alkaline environment has a greater influence on the late strength of cement (7–28 days).
2) The species of hydration products of OPC did not change under different pH maintenance conditions, and they were still AFt, AFm, CH. However, the pH value had an effect on the content of different hydration products. With the increase of pH, the content of CH increased significantly, but the content of AFt was the most abundant in neutral environment.
3) The morphologies of hydration products of solutions with different pH values are obviously different. In acidic solution, C-S-H gel is cloudy with well-crystallized ettringite columnar crystals nearby. In alkaline solution, C-S-H is fibrous and ettringite is small needle rod and grows radially outward.
4) By considering the solid/liquid interface in the cement paste, the heterogeneity of hydration products and the uneven charge space distribution in the matrix, the newly proposed equivalent circuit $R_s(Q_1R_{ct1}(Q_2R_{ct2})W_1$ is established. The calculated parameters of R_{ct} with pH = 12 shows a trend of rising and then declining as the curing age prolongs, different from the increasing trends of R_{ct} with pH = 3 and 7.
5) There is an obvious logarithmic relation between the electrochemical parameter of R_{cp} and compressive strength of hardened cement paste. The fitting coefficients (R^2) of mathematical relation is more than 90%. According to in-site monitoring EIS of cement system, the matrix compressive strength can be quantitatively predicted.

Data availability statement

The raw data supporting the conclusion of this article will be made available by the authors, without undue reservation.

Author contributions

All authors listed have made a substantial, direct, and intellectual contribution to the work and approved it for publication.

Funding

The financial help is supported by the National Natural Science Foundation of China (No.52078192, 52078332 and U2006223), Henan Natural Science Foundation

(No.212300410043) and Henan Province Basic Research Program (No.21A430018).

Conflict of interest

The authors declare that the research was conducted in the absence of any commercial or financial relationships that could be construed as a potential conflict of interest.

Publisher's note

All claims expressed in this article are solely those of the authors and do not necessarily represent those of their affiliated organizations, or those of the publisher, the editors and the reviewers. Any product that may be evaluated in this article, or claim that may be made by its manufacturer, is not guaranteed or endorsed by the publisher.

References

Bentz, D. P. (2006). Influence of alkalis on porosity percolation in hydrating cement pastes. *Cem. Concr. Compos.* 28 (5), 427–431. doi:10.1016/j.cemconcomp.2006.01.003

Bertron, A., Duchesne, J., and Escadeillas, G. (2005). Accelerated tests of hardened cement pastes alteration by organic acids: Analysis of the pH effect. *Cem. Concr. Res.* 35 (1), 155–166. doi:10.1016/j.cemconres.2004.09.009

Cabeza, M., Merino, P., Miranda, A., Nóvoa, X. R., and Sanchez, I. (2002). Impedance spectroscopy study of hardened Portland cement paste. *Cem. Concr. Res.* 32, 881–891. doi:10.1016/s0008-8846(02)00720-2

Chi, L., Wang, Z., Lu, S., Zhao, D., and Yao, Y. (2019). Development of mathematical models for predicting the compressive strength and hydration process using the EIS impedance of cementitious materials. *Constr. Build. Mater.* 208, 659–668. doi:10.1016/j.conbuildmat.2019.03.056

Cruz, J. M., Fita, I. C., Soriano, L., Payá, J., and Borrachero, M. V. (2013). The use of electrical impedance spectroscopy for monitoring the hydration products of Portland cement mortars with high percentage of pozzolans. *Cem. Concr. Res.* 50, 51–61. doi:10.1016/j.cemconres.2013.03.019

De Weerdt, K., and Justnes, H. (2015). The effect of sea water on the phase assemblage of hydrated cement paste. *Cem. Concr. Compos.* 55, 215–222. doi:10.1016/j.cemconcomp.2014.09.006

De Windt, L., and Devillers, P. (2010). Modeling the degradation of Portland cement pastes by biogenic organic acids. *Cem. Concr. Res.* 40 (8), 1165–1174. doi:10.1016/j.cemconres.2010.03.005

Diamond, S. (2000). Mercury porosimetry: An inappropriate method for the measurement of pore size distributions in cement-based materials. *Cem. Concr. Res.* 30, 15–17. doi:10.1016/S0008-8846(00)00370-7

Diamond, S. (2000). Microscopic features of ground water induced sulfate attack in highly permeably concretes. *Concr. Inst.* 192, 403–416.

Dong, B., Li, G., Zhang, J., Liu, Y., Xing, F., and Hong, S. (2017). Non-destructive tracing on hydration feature of slag blended cement with electrochemical method. *Constr. Build. Mater.* 149, 467–473. doi:10.1016/j.conbuildmat.2017.05.042

Dong, B., Qiu, Q., Gu, Z., Xiang, J., Huang, C., Fang, Y., et al. (2016). Characterization of carbonation behavior of fly ash blended cement materials by the electrochemical impedance spectroscopy method. *Cem. Concr. Compos.* 65, 118–127. doi:10.1016/j.cemconcomp.2015.10.006

Dong, B., Wu, Y., Teng, X., Zhuang, Z., Gu, Z., Zhang, J., et al. (2019). Investigation of the Cl− migration behavior of cement materials blended with fly ash or/and slag via the electrochemical impedance spectroscopy method. *Constr. Build. Mater.* 211, 261–270. doi:10.1016/j.conbuildmat.2019.03.198

Dove, P. M. (1999). The dissolution kinetics of quartz in aqueous mixed cation solutions. *Geochimica Cosmochimica Acta* 63 (22), 3715–3727. doi:10.1016/s0016-7037(99)00218-5

Gong, K., and White, C. E. (2018). Nanoscale chemical degradation mechanisms of sulfate attack in alkali-activated slag. *J. Phys. Chem. C* 122, 5992–6004. doi:10.1021/acs.jpcc.7b11270

Grutzeck, M. W. (1999). A new model for the formation of calcium silicate hydrate (C-S-H). *Mater. Res. innovations* 3 (3), 160–170. doi:10.1007/s100190050143

Guo, H., Liu, Y., Tai, B., Zhang, Z., and Zhu, Y. (2022). Effect of environmental pH value on mechanical properties and microstructure of hardened sulphoaluminate cement paste. *Constr. Build. Mater.* 325, 126848. doi:10.1016/j.conbuildmat.2022.126848

Guo, T., Wu, T., Gao, L., He, B., Ma, F., Huang, Z., et al. (2021). Compressive strength and electrochemical impedance response of red mud-coal metakaolin geopolymer exposed to sulfuric acid. *Constr. Build. Mater.* 303, 124523. doi:10.1016/j.conbuildmat.2021.124523

Gutberlet, T., Hilbig, H., and Beddoe, R. E. (2015). Acid attack on hydrated cement - effect of mineral acids on the degradation process. *Cem. Concr. Res.* 74, 35–43. doi:10.1016/j.cemconres.2015.03.011

Hassi, S., Ebn Touhami, M., Boujad, A., and Benqlilou, H. (2020). Assessing the effect of mineral admixtures on the durability of Prestressed Concrete Cylinder Pipe (PCCP) by means of electrochemical impedance spectroscopy. *Constr. Build. Mater.* 262, 120925. doi:10.1016/j.conbuildmat.2020.120925

He, F., Wang, R., Shi, C., Zhang, R., Chen, C., Lin, L., et al. (2017). Differential analysis of AC impedance spectroscopy of cement-based materials considering CPE behavior. *Constr. Build. Mater.* 143, 179–188. doi:10.1016/j.conbuildmat.2017.03.119

He, H., Zhu, Y., and Zhou, A. (2018). Electrochemical impedance spectroscopy (EIS) used to evaluate influence of different external pressures, curing ages and self-healing environments on the self-healing behavior of engineered cementitious composites (ECC). *Constr. Build. Mater.* 188, 153–160. doi:10.1016/j.conbuildmat.2018.08.104

Hernandez-Vargas, G., Sosa-Hernández, J., Saldarriaga-Hernandez, S., Villalba-Rodríguez, A., Parra-Saldivar, R., and Iqbal, H. (2018). Electrochemical biosensors: A solution to pollution detection with reference to environmental contaminants. *Biosensors* 8, 29. doi:10.3390/bios8020029

Hu, X., Shi, C., Liu, X., Zhang, J., and de Schutter, G. (2019). A review on microstructural characterization of cement-based materials by AC impedance spectroscopy. *Cem. Concr. Compos.* 100, 1–14. doi:10.1016/j.cemconcomp.2019.03.018

Ismail, I., Bernal, S. A., Provis, J. L., Hamdan, S., and van Deventer, J. S. J. (2013). Drying-induced changes in the structure of alkali-activated pastes. *J. Mat. Sci.* 48, 3566–3577. doi:10.1007/s10853-013-7152-9

Jain, J., and Neithalath, N. (2011). Electrical impedance analysis based quantification of microstructural changes in concretes due to non-steady state chloride migration. *Mater. Chem. Phys.* 129, 569–579. doi:10.1016/j.matchemphys.2011.04.057

Juenger, M. C. G., and Jennings, H. M. (2001). Effects of high alkalinity on cement pastes. *Mater. J.* 98, 251–255.

Juenger, M. C. G., and Jennings, H. M. (2001). Effects of high alkalinity on cement pastes. *ACI Mat. J.* 98 (3), 251–255.

Kazemian, S., Prasad, A., Bolouri Bazaz, B. J., Mohammed, T. A., and Abdul Aziz, F. N. (2011). Effect of aggressive pH media on peat treated by cement and sodium silicate grout. *J. Cent. South Univ. Technol.* 18, 840–847. doi:10.1007/s11771-011-0771-x

Kong, L., Hou, L., and Bao, X. (2015). Application of AC impedance technique in study of lightweight aggregate-paste interface. *Constr. Build. Mater.* 82, 332–340. doi:10.1016/j.conbuildmat.2015.02.079

Kong, L., Hou, L., Wang, Y., and Sun, G. (2016). Investigation of the interfacial transition zone between aggregate-cement paste by AC impedance spectroscopy. *J. Wuhan. Univ. Technol.-Mat. Sci. Ed.* 31, 865–871. doi:10.1007/s11595-016-1460-2

Li, G., Zhang, A., Song, Z., Shi, C., Wang, Y., and Zhang, J. (2017). Study on the resistance to seawater corrosion of the cementitious systems containing ordinary Portland cement or/and calcium aluminate cement. *Constr. Build. Mater.* 157, 852–859. doi:10.1016/j.conbuildmat.2017.09.175

Li, Y., Peng, W., Guan, Z. Z., and Ding, Q. J. (2017). Micro-mechanical properties of individual phases in cement pastes under brine solution using nanoindentation and scanning electron microscopy. *JNanoR* 46, 31–44. doi:10.4028/www.scientific.net/jnanor.46.31

Li, Y., Zhang, G., Wang, Z., Wang, P., and Guan, Z. (2018). Integrated experimental-computational approach for evaluating elastic modulus of cement

paste corroded in brine solution on microscale. *Constr. Build. Mater.* 162, 459–469. doi:10.1016/j.conbuildmat.2017.12.075

Liu, X., Feng, P., Li, W., Geng, G., Huang, J., Gao, Y., et al. (2021). Effects of pH on the nano/micro structure of calcium silicate hydrate (C-S-H) under sulfate attack. *Cem. Concr. Res.* 140, 106306. doi:10.1016/j.cemconres.2020.106306

Lloyd, R. R., Provis, J. L., and van Deventer, J. S. J. (2009). Microscopy and microanalysis of inorganic polymer cements. 1: Remnant fly ash particles. *J. Mat. Sci.* 44, 608–619. doi:10.1007/s10853-008-3077-0

Mohit, M., Ranjbar, A., and Sharifi, Y. (2021). Mechanical and microstructural properties of mortars incorporating ceramic waste powder exposed to the hydrochloric acid solution. *Constr. Build. Mater.* 271, 121565. doi:10.1016/j.conbuildmat.2020.121565

Muthu, M., Yang, E., and Unluer, C. (2021). Resistance of graphene oxide-modified cement pastes to hydrochloric acid attack. *Constr. Build. Mater.* 273, 121990. doi:10.1016/j.conbuildmat.2020.121990

Okohira, K., Sato, N., and Mori, H. (1974). Observation of three-dimensional shapes of inclusions in low-carbon aluminum-killed steel by scanning electron microscope. *ISIJ Int.* 14 (2), 102–109. doi:10.2355/isijinternational1966.14.102

Ortega, J. M., Sánchez, I., and Climent, M. A. (2015). Impedance spectroscopy study of the effect of environmental conditions in the microstructure development of OPC and slag cement mortars. *Archives Civ. Mech. Eng.* 15, 569–583. doi:10.1016/j.acme.2014.06.002

Paglia, C., Wombacher, F., and Böhni, H. (2003). The influence of alkali-free and alkaline shotcrete accelerators within cement systems. *Cem. Concr. Res.* 33 (3), 387–395. doi:10.1016/s0008-8846(02)00967-5

Paul, G., Boccaleri, E., Buzzi, L., Canonico, F., and Gastaldi, D. (2015). Friedel's salt formation in sulfoaluminate cements: A combined XRD and 27 Al mas nmr study. *Cem. Concr. Res.* 67, 93–102. doi:10.1016/j.cemconres.2014.08.004

Ramachandran, V., Beaudoin, J., Sarkar, S., and Xu, A. (1993). Physico-chemical and microstructural investigations of the effect of NaOH on the hydration of $3CaO{\cdot}SiO_2$. *Cement* 1993, 73–90.

Ramu, Y. K., Sirivivatnanon, V., Thomas, P., Dhandapani, Y., and Vessalas, K. (2021). Evaluating the impact of curing temperature in delayed ettringite formation using electrochemical impedance spectroscopy. *Constr. Build. Mater.* 282, 122726. doi:10.1016/j.conbuildmat.2021.122726

Renaudin, G., Russias, J., Leroux, F., Cau-dit-Coumes, C., and Frizon, F. (2009). Structural characterization of C-S-H and C-A-S-H samples-Part II: Local environment investigated by spectroscopic analyses. *J. Solid State Chem.* 182 (12), 3320–3329. doi:10.1016/j.jssc.2009.09.024

Ribeiro, D. V., and Abrantes, J. C. C. (2016). Application of electrochemical impedance spectroscopy (EIS) to monitor the corrosion of reinforced concrete: A new approach. *Constr. Build. Mater.* 111, 98–104. doi:10.1016/j.conbuildmat.2016.02.047

Shayan, S. J. W. A. (1989). Early hydration of a portland cement in water and sodium hydroxide solutions: Composition of solutions and nature of solid phases. *Cem. Concr. Res.* 19 (5), 759–769.

Shimada, Y., and Young, J. F. (2004). Thermal stability of ettringite in alkaline solutions at 80 °C. *Cem. Concr. Res.* 34 (12), 2261–2268. doi:10.1016/j.cemconres.2004.04.008

Silva, Y. F., and Delvasto, S. (2021). Sulfate attack resistance of self-compacting concrete with residue of masonry. *Constr. Build. Mater.* 268, 121095. doi:10.1016/j.conbuildmat.2020.121095

Snyder, K. A., Feng, X., Keen, B. D., and Mason, T. O. (2003). Estimating the electrical conductivity of cement paste pore solutions from OH−, K+ and Na+ concentrations. *Cem. Concr. Res.* 33 (6), 793–798. doi:10.1016/s0008-8846(02)01068-2

Song, G. (2000). Equivalent circuit model for AC electrochemical impedance spectroscopy of concrete. *Cem. Concr. Res.* 30, 1723–1730. doi:10.1016/s0008-8846(00)00400-2

Spragg, R. P., Villani, C., and Weiss, J. (2014). Surface and uniaxial electrical measurements on layered cementitious composites having cylindrical and prismatic geometries. *Int. Conf. Durab. Concr. Struct.*, 317–326. doi:10.5703/1288284315417

Tang, S. W., Zhu, H. G., Li, Z. J., Chen, E., and Shao, H. Y. (2015). Hydration stage identification and phase transformation of calcium sulfoaluminate cement at early age. *Constr. Build. Mater.* 75, 11–18. doi:10.1016/j.conbuildmat.2014.11.006

Taylor, H. F. W., Famy, C., and Scrivener, K. L. (2001). Delayed ettringite formation. *Cem. Concr. Res.* 31, 683–693. doi:10.1016/s0008-8846(01)00466-5

Thomas, J. J., Biernacki, J. J., Bullard, J. W., Bishnoi, S., Dolado, J. S., Scherer, G. W., et al. (2011). Modeling and simulation of cement hydration kinetics and microstructure development. *Cem. Concr. Res.* 41, 1257–1278. doi:10.1016/j.cemconres.2010.10.004

Tteardon, C. J. W. A. (1994). The solubility of ettringite at 25oC. *Cem. Concr. Res.* 24 (8), 1515–1524.

Wang, X., Pan, Z., Shen, X., and Liu, W. (2016). Stability and decomposition mechanism of ettringite in presence of ammonium sulfate solution. *Constr. Build. Mater.* 124, 786–793. doi:10.1016/j.conbuildmat.2016.07.135

Wei, X., Xiao, L., and Li, Z. (2012). Prediction of standard compressive strength of cement by the electrical resistivity measurement. *Constr. Build. Mater.* 31, 341–346. doi:10.1016/j.conbuildmat.2011.12.111

Wilińska, I., and Pacewska, B. (2018). Influence of selected activating methods on hydration processes of mixtures containing high and very high amount of fly ash. *J. Therm. Anal. Calorim.* 133, 823–843. doi:10.1007/s10973-017-6915-y

Xue, J., Liu, S., Ma, X., Teng, Y., and Guan, X. (2022). Effect of different gypsum dosage on the chloride binding properties of C4AF hydrated paste. *Constr. Build. Mater.* 315, 125562. doi:10.1016/j.conbuildmat.2021.125562

Yan, X., Jiang, L., Guo, M., Chen, Y., Jiang, S., and Song, S. (2020). A nondestructive EIS method to evaluate the compressive strength of slag-blended cement paste under steam curing. *J. Test. Eval.* 48, 4104–4115. doi:10.1520/jte20180259

Yang, Y., Ji, T., Lin, X., Chen, C., and Yang, Z. (2018). Biogenic sulfuric acid corrosion resistance of new artificial reef concrete. *Constr. Build. Mater.* 158, 33–41. doi:10.1016/j.conbuildmat.2017.10.007

Zhang, G., Wu, C., Hou, D., Yang, J., Sun, D., and Zhang, X. (2021). Effect of environmental pH values on phase composition and microstructure of Portland cement paste under sulfate attack. *Compos. Part B Eng.* 216, 108862. doi:10.1016/j.compositesb.2021.108862

Zhang, W., Zhang, J., Ye, J., Wang, H., and Liu, J. (2017). Influence of synthesis conditions on morphology of ettringite. *J. Chin. Ceram. Soc.* 45 (05), 631–638. doi:10.14062/j.issn.0454-5648.2017.05.05

Zhu, Y., Zhang, H., Zhang, Z., and Yao, Y. (2017). Electrochemical impedance spectroscopy (EIS) of hydration process and drying shrinkage for cement paste with W/C of 0.25 affected by high range water reducer. *Constr. Build. Mater.* 131, 536–541. doi:10.1016/j.conbuildmat.2016.08.099

Zivica, V., and Bajza, A. (2002). Acidic attack of cement-based materials-a review Part 2. Factors of rate of acidic attack and protective measures. *Constr. Build. Mater.* 16, 215–222. doi:10.1016/s0950-0618(02)00011-9